Multiphysics Modeling Methodology for Radiofrequency Tissue Ablation

Joshua M. Thomas[1], Jeffrey S. Crompton*[1], and Kyle C. Koppenhoefer[1]
1. AltaSim Technologies, LLC 130 E. Wilson Bridge Rd, Suite 140, Columbus, OH, 43085
*Corresponding author: jeff@altasimtechnologies.com

Abstract: This paper describes the development of a multiphysics-based computational modeling methodology for radiofrequency tissue ablation (RFA). The general methodology is also applied to the specific case of blood vessel wall ablation. The model has been used to isolate the effect of critical parameters and thermal mechanisms on the successful operation of the device.

Keywords: radiofrequency ablation, tissue ablation, necrosis, multiphysics, Joule heating, bioheat transfer, mechanical contact

1. Introduction

Necrosis of human tissue can be obtained by exposure to temperatures below 40°C or above +50°C. However, inherent variability in tissue properties, the complexity of tissue response and dissipation of thermal energy by local perfusion and blood flow can make the development of routine, predictable in-vivo approaches to obtain necrosis difficult. Although a number of thermal ablation techniques exist, optimization of electrode design and operational practices is difficult using traditional in-vivo or in-vitro based testing. To overcome these limitations computational analysis has been used to simulate device performance and enable the development of safer operating procedures and instrument designs.

For ablation technology in which a current carrying electrode is inserted into a blood vessel and pressed against the vessel wall, deformation of the tissue can occur that changes the degree of local contact and thus affects the efficiency of heat transfer into the surrounding tissue. To obtain efficient tissue ablation, mechanical contact must be maintained between the ablation electrode and the site of interest (see Figure 1). In addition, local perfusion and blood flow can lead to increased dissipation of thermal energy. In this work, COMSOL Multiphysics® has been used to simulate the coupled effects of changing mechanical contact with the vessel wall during deformation, laminar fluid flow due to blood flow through the vessel, bioheat transfer due to perfusion in the surrounding tissue and flow of electric current in the electrode to produce Joule heating.

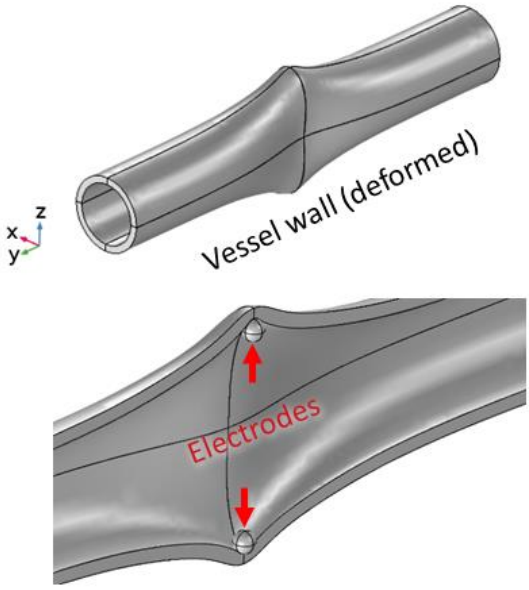

Figure 1. Deformed vessel wall (top) with cut-away view of vessel with spherical electrodes pressing against the vessel wall.

2. Computational Model & Governing Equations

The multiphysics-based computational model includes the following sets of equations and implementation using COMSOL Multiphysics®:

1. Solid Mechanics with contact
2. Laminar flow
3. Electric currents
4. Heat Transfer with perfusion (Bioheat transfer)

The physical steps taken in the use of the ablation device are juxtaposed with the computational model actions in Table 1.

Table 1: Multiphysics implementation

	Physical action	**Numerical model action**
Step 1	Insert electrode into vessel and press against vessel wall	Solve Solid Mechanics with contact
		Export/import deformed geometry
		Solve Laminar Flow
Step 2	Turn on electrode voltage	Solve Electric Currents
		Solve Heat Transfer

The solid mechanics governing equations for a linear elastic material (1), a linear constitutive model (2), and a linear strain-displacement relationship (3) are used.

$$\nabla \cdot \sigma = \mathbf{0}, \tag{1}$$

$$\boldsymbol{S} = \mathbf{C} : \varepsilon \tag{2}$$

$$\varepsilon = \frac{1}{2}(\nabla \mathbf{u} + (\nabla \mathbf{u})^{\mathbf{T}}) \tag{3}$$

The Augmented Lagrangian contact pressure method available with the Structural Mechanics module is used. The default solver settings are used with the "Force Linear Strains" setting in the Linear Elastic Material model to override the geometric non-linearity setting required by the contact formulation. This setting helps with more robust convergence at the sacrifice of some accuracy in strain-displacement calculation at higher displacements.

Vessel ends are constrained with a fixed constraint displacement boundary condition at a distance of 5X the diameter of the vessel to avoid boundary effects.

In the fluid domain, the flow physics are described by the conversation of mass and momentum equations.

$$\nabla \cdot (\rho\, \mathbf{u}) = 0 \tag{4}$$

$$\rho\, \mathbf{u} \cdot \nabla \mathbf{u} = -\nabla p + \nabla \cdot \left(\eta\left(\nabla \mathbf{u} + (\nabla \mathbf{u})^{T}\right) - \frac{2}{3}\eta(\nabla \cdot \mathbf{u})\mathbf{I} \right) \tag{5}$$

Flow inlet velocity is applied as 60 cm/s average blood flow at a distance of 5X the diameter of the vessel upstream of the electrode (see Figure 2).

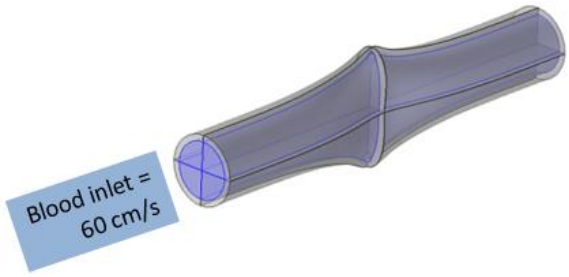

Figure 2. Flow domain in blue with inlet flow boundary condition defined as 60 cm/s average velocity.

The electric current conservation and constitutive equations are used in all domains.

$$\nabla \cdot \mathbf{J} = 0 \tag{6}$$

$$\nabla \cdot \mathbf{J} = \mathbf{E} \tag{7}$$

$$\mathbf{E} = -\nabla \mathrm{V} \tag{8}$$

Ground boundary conditions are applied to all surfaces of the block tissue modeling volumes. A point voltage of 14 V is applied to the center of the spherical electrodes. Figure 3 shows the block tissue encasing the vessel.

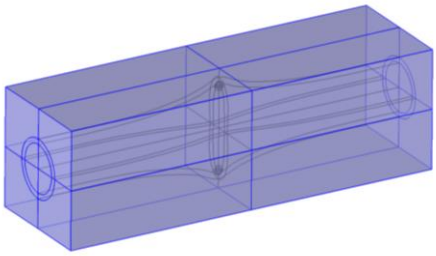

Figure 3. Vessel enclosed in a block of tissue. Ground (V=0) boundary condition applied to the surfaces of the block.

The heat transfer equation is used in both fluid and solid domains.

$$\nabla \cdot (-k\nabla T) = Q - \rho\, c_p \mathbf{u} \tag{9}$$

Where Q is the heat source term with contributions from Joule heating, $Q_e = \mathbf{J} \cdot \mathbf{E}$, adding heat and the

blood perfusion equations, $Q_p = \rho_b * C_{p,b} * \omega_b(T_b - T)$.
A body temperature boundary condition of 37°C is applied at the boundaries that are electrically grounded.

A 1/8 symmetry solid mechanics solution is obtained with a custom mapped and swept mesh with ~10 elements through the vessel thickness for the vessel domain and 0.03 mm maximum element size for the spherical electrode (free tetrahedral). The fine mesh is used for the contact/displacement solution for extra precision in the deformed geometry representation. The 1/8 symmetric deformed geometry is mirrored 3 times across appropriate planes to reconstitute the full 3D geometry for subsequent solver steps. This full 3D geometry (with no symmetry assumptions) is used to solve for the remaining physics variables using the default "Physics-controlled" mesh at "Finer" element size parameters.

All equations are solved in the stationary equation form with default solver settings.

3. Results

One of the purposes of this study is to determine the effect of critical variables and physical phenomena on system performance. A comparison of the temperature field without deformation in the "flow" and "no flow" scenarios is compared (Figure 4).

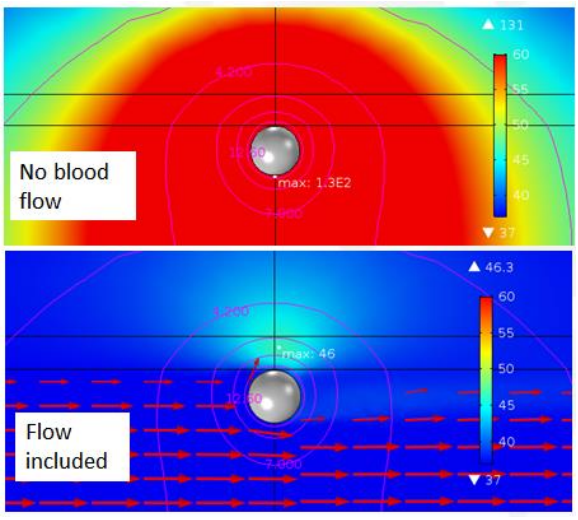

Figure 4. Temperature (°C) slice plots under no flow (top) and flow (bottom) conditions for the case where no deformation is considered. Flow arrows (red) and voltage contours (magenta) are also included for reference.

The large difference in these solutions indicates that heat transfer due to blood flow is significant in predicting the temperature distribution.

During use, local deformation of the vessel walls occurs which can affect the local flow. Figures 5 and 6 show velocity slice plots and cut line plots of the difference between the undeformed and deformed (electrode displacement = 2.32 mm) velocity field in the region near the electrode.

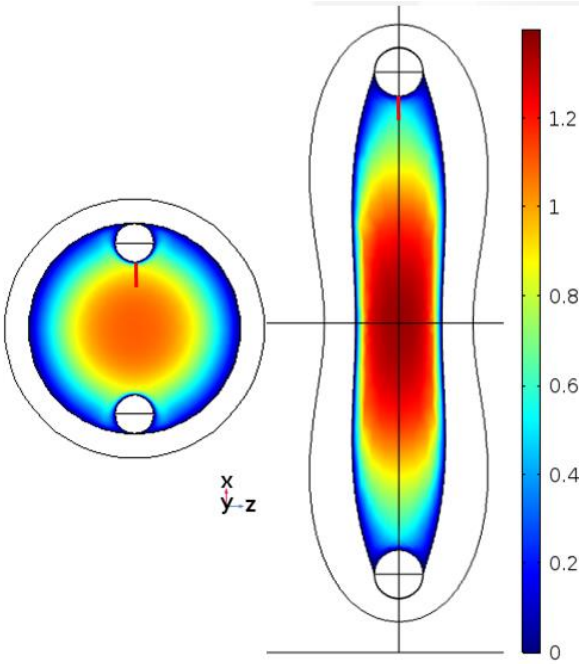

Figure 5. Velocity field slice plots (m/s) in the undeformed (left) and deformed (right) configurations. Electrode displacement is 2.32 mm in the deformed case. Red cut lines define arc length in Figure 6.

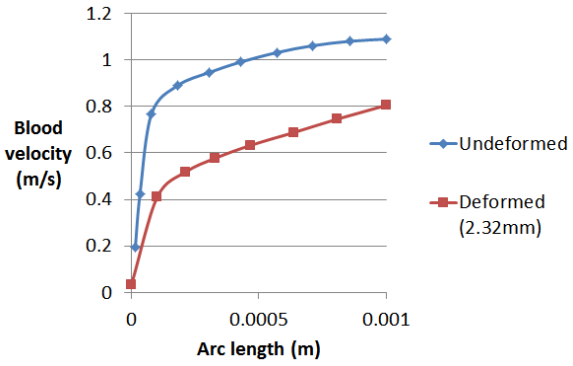

Figure 6. Blood velocity (m/s) vs arc length of cut lines defined in Figure 5.

The flow field solution in the region of deformation is highly dependent (~33% difference) on the deformed shape. The effect of the deformation

induced blood flow on the temperature distribution can be seen in Figure 7.

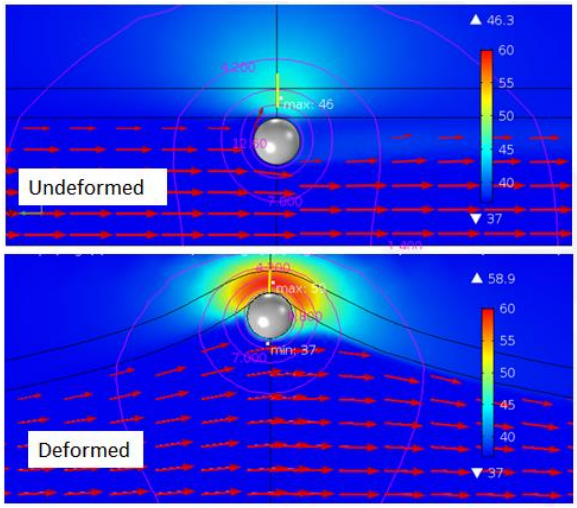

Figure 7. Temperature slice plots (°C) of the undeformed and deformed solutions (electrode displacement = 2.32 mm). Flow arrows and voltage contours are also included for reference. Yellow cut lines through the thickness of the vessel define arc lengths for Figure 8.

The large temperature difference (~15°C) indicates that including the effect of deformed tissue shape is important for accurate temperature prediction in this type of problem where convective heat transfer into the flow stream is affected by the change in vessel shape. The effect on subsequent tissue necrosis can be seen in Figure 8. Assuming that tissue necrosis occurs at temperatures above 50°C, it can be seen that failing to include vessel deformation would predict no necrosis whereas the deformed case predicts complete necrosis through the thickness of the vessel.

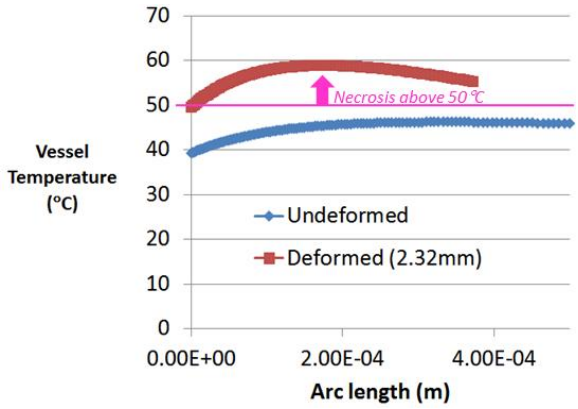

Figure 8. Through-thickness temperature for the vessel in the undeformed and deformed cases.

The effect blood perfusion in the bulk tissue is shown in Figure 9. Based on the 50°C cut-off criterion the predicted volume of tissue experiencing a temperature in excess of 50°C is 0.0035 cm^3 compared to 0.0033 cm^3, a difference of about 5%.

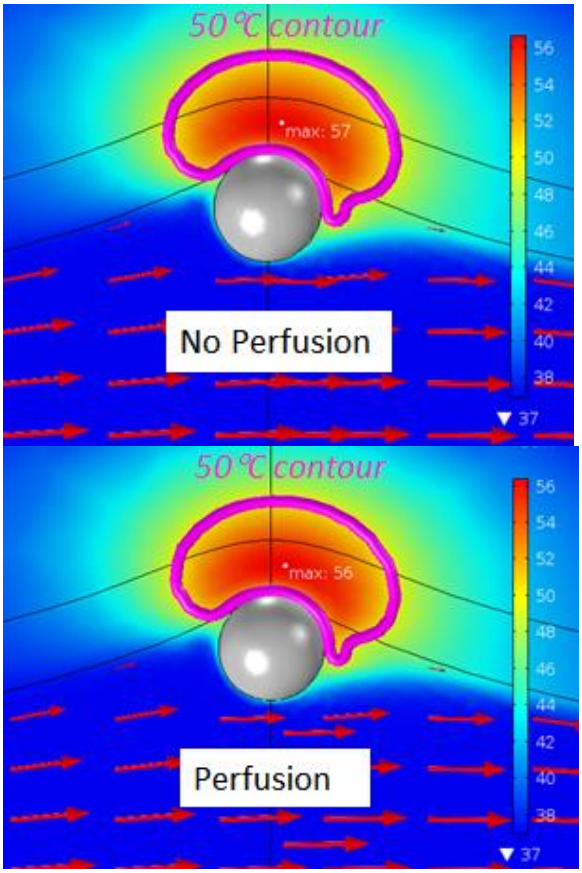

Figure 9. Temperature solution (°C) with and without bulk tissue perfusion included. The difference in volume of tissue experiencing necrosis is about 5%.

4. Conclusions

A computational model of a radiofrequency based tissue ablation system has been implemented in COMSOL Multiphysics® . The model has identified critical factors associated with use of radiofrequency based ablation technology. Accurately prediction of tissue necrosis requires that the effects of local tissue deformation of the vessel wall and blood flow through the vessel are included. Of secondary importance is the inclusion of the effects of blood perfusion in the surrounding tissue.

5. References

Frei, Walter, *Study Radiofrequency Tissue Ablation Using Simulation*, COMSOL Blog, https://www.comsol.com/blogs/study-radiofrequency-tissue-ablation-using-simulation/, posted Jan. 20, 2016.